J Mater Sci (2016) 51:7780–7792

Formation mechanisms and evolution of precipitate-free zones at grain boundaries in an Al–Cu–Mg–Mn alloy during homogenisation

Y. Q. Chen[1,*], S. P. Pan[2], S. W. Tang[1], W. H. Liu[1], C. P. Tang[1], and F. Y. Xu[3]

[1] *Hunan Provincial Key Defense Laboratory of High Temperature Wear-Resisting Materials and Preparation Technology, Hunan University of Science and Technology, Xiangtan 411201, People's Republic of China*
[2] *Advanced Research Center, Central South University, Changsha 410083, People's Republic of China*
[3] *School of Mechanical Engineering, Xiangtan University, Xiangtan 411105, People's Republic of China*

Received: 29 February 2016
Accepted: 11 May 2016
Published online: 18 May 2016

ABSTRACT

Solute and vacancy depletion have long been investigated to reveal the formation mechanism of grain boundary precipitate-free zones (GB-PFZ) during ageing, yet there is no conclusive explanation due to the simultaneous appearance of the two in GB-PFZ. In this study, the evolution of GB-PFZs and solute distributions in the vicinity of grain boundaries (GBs) were studied during the homogenisation of an Al–Cu–Mg–Mn alloy using transmission electron microscopy, high-angle annular dark field scanning transmission electron microscopy, and energy-dispersive X-ray spectroscopy. Results indicated that the evolution of GB-PFZ during homogenisation can be divided into the following three stages: Stage I, formation and recession of GB-PFZ; Stage II, absence of GB-PFZ, and Stage III, the reappearance and broadening of GB-PFZ. The results also revealed that the GB-PFZ in Stage I is totally devoid of solute depletion and its formation can be attributed to vacancy depletion alone. The GB-PFZ at Stage III solely caused by solute depletion and excludes vacancy depletion.

Introduction

Precipitation hardening is one of the most important strengthening techniques used on Al-based alloys [1]. Its main principle is to produce a homogeneous distribution of fine precipitates in the alloy which provides barriers to dislocation motion [2]. However, owing to performance differences between GB and the matrix, inhomogeneous distributions of precipitates always exist in the vicinity of GBs [3, 4]. A very noticeable feature is the existence of "precipitate-free zones" (PFZs) [5, 6].

Generally, PFZs are thought to be "weak zones" in an alloy, since they are free of precipitates and softer than other regions in the matrix. Further studies revealed that the mechanical behaviour, fracture

Address correspondence to E-mail: yqchen1984@163.com

DOI 10.1007/s10853-016-0062-x

resistance, and stress corrosion cracking resistance of alloys had a close relationship with PFZ features [5, 6]. Therefore, the formation mechanism and evolution of PFZs have become hot topics in materials science.

Previous studies on PFZ formation mainly focused on the ageing process. It was revealed that the PFZ always appears at the same time as inner grain precipitation [10] and its width constantly increases with age [11–13]. Two mechanisms were put forward to account for PFZ formation: vacancy depletion and solute depletion. The vacancy depletion mechanism takes the effects of vacancy sinks during quenching into account, which results in retarded precipitation around GBs compared with that in the inner grain [11]. Under the solute depletion mechanism, the suppressed precipitation around GBs is attributed to the decreased supersaturation of solute atoms, which is frequently induced in conjunction with the formation of more stable, coarsened GB precipitates [12].

Although the mechanisms of vacancy depletion and solute depletion are now widely accepted, it remains unclear as to whether only one mechanism individually, or both collectively, lead to the formation of PFZs [11]. There has been no evidence for one mechanism to function alone in the ageing process. For example, vacancy depletion is considered to be the dominant mechanism in the early stage of GB-PFZ formation; however, a certain level of solute depletion induced by the preferential precipitation at GBs can still be detected [12–14]. Besides, at the later stage of ageing in which the solute depletion mechanism is considered to be dominant in GB-PFZ formation [15], severe vacancy depletion may also exist because of the constant consumption of vacancies by the precipitation [16, 17].

Besides those seen at GBs, the formation of PFZs has been widely observed at the interface region of the matrix and reinforcement particles or fibres in several different ages of different alloys [18–20]. Recently, GB-PFZs were also observed in some Al alloys during homogenisation [21, 22] but unfortunately have not drawn enough attention, probably due to less technical interest. In particular, more studies are required to better understand the formation mechanism of GB-PFZs. In our previous study [23], the simultaneous formation of two PFZs during the initial stage of homogenisation in an Al alloy was first observed with one near GBs and the other at the grain centres (GC-PFZ). Microstructural analyses indicated that the formations of these two types of PFZs might be due solely to solute and vacancy depletion, respectively.

In this study, a systematic investigation on the precipitation behaviour of an alloy near GB regions during homogenisation was carried out. The main objectives were to reveal the mechanisms underpinning the formation and evolution of GB-PFZ during homogenisation, and better understand the formation mechanism of PFZ.

Experimental conditions

The material used in this study was a 2524 alloy provided by Northeast Light Alloy Co. Ltd with chemical compositions of 1.92 % Cu, 1.71 % Mg, 0.22 % Mn, 0.03 % Fe, 0.06 % Si, and Al (the remainder) (all in at.%). All samples were taken from the mid-radius of the cast ingot (∅120 × L200 mm) and cut to sheets measuring 10 mm × 10 mm × 1 mm. Homogenisation annealing was performed in an electric furnace at 485 °C for a series of designed holding times followed by water quenching.

Transmission electron microscopy (TEM) and high-angle annular dark field scanning transmission electron microscopy (HAADF-STEM) analyses were then performed using a FEI Tecnai G^2 F 20 electron microscope operated at 200 kV. Electrolytic polishing was conducted using an electrolyte composed of 25 % nitric acid and 75 % methanol at −25 °C.

For the measurement of the PFZ widths, at least 10 different GBs were investigated for each homogenisation condition. The PFZ width was measured as the average shortest distance between the GB and five nearest precipitates/dispersoids. Care was taken to align the grain boundaries so that they were parallel to the electron beam direction, so that a true width of the PFZ was acquired. The solute concentrations in the matrix were assessed by using energy-dispersive X-ray spectroscopy (EDX, INCA Energy 200, Oxford Instruments) with a probe size of 80 nm. Inside the precipitation area, EDX was performed between precipitates, with a spacing of at least 200 nm between scans. Five measurements were taken and the average values and standard deviation were reported as individual data points in the solute concentration curve. The horizontal error bar represents the probe size considering beam spreading in the sample.

It was revealed that the measurement of Cu concentration exhibits an apparent dependence on the foil thickness in regions of <200 nm thickness, due to redeposition of Cu on the surface during electropolishing [24]. This effect decreased rapidly with increasing foil thickness and it no longer influenced the measured Cu content for foil thicknesses in excess of 200 nm [24, 25]. For this reason, the results from regions measuring 200–250 nm in thickness were analysed. The foil thickness was measured by counting thickness fringes at $s = 0$, and by measuring the separation between contamination spots [25].

During EDX analysis, all the X-ray spectra were generated for a fixed Al $K\alpha$ peak integrated intensity of 20,000 counts in the samples. The collected spectra were quantified through an analysis software package, Desktop Spectra Analyser (DTSA). The counting time varied within the range 90–110 s depending on sample thickness. To test the accuracy of the K values used in the analysis, the sample homogenised at 485 °C for 30,000 min was used as a standard. X-ray spectra were generated from the centre of the grains using EDX in TEM.

The X-ray intensities used in this study are integrated intensities (I) of the characteristic $K\alpha$ X-ray peaks, corrected for background intensity.

The concentration ratios were calculated from the measured intensity ratios using the Cliff–Lorimer method, which for elements A and B, are formally described by the equation [24]:

$$\frac{I_A}{I_B} = k\frac{C^A}{C^B} \quad [24], \tag{1}$$

where I_A and I_B are the intensities of the characteristic X-ray peaks of A and B, C_A and C_B are the concentrations of A and B (by weight fraction), and k is the Cliff–Lorimer factor. The value of k was found to be independent of foil thickness (t) and concentration in this study. Therefore, it was considered as a constant. This criterion considers only the effect of X-ray absorption, and is stated as [13]:

$$\frac{1}{2}(\chi_B - \chi_A)\rho t < 0.1 \quad [13], \tag{2}$$

where

$$\chi = \frac{\rho}{\mu}\csc\alpha \quad [13] \tag{3}$$

ρ/μ is the mass absorption coefficient, ρ is the density, and α is the take-off angle.

Experimental results

Figure 1a shows a typical TEM image of the as-cast alloy obtained from the <010> zone axis of Al matrix. In agreement with previous observations [23], no precipitates were observed within grain interiors. This can be also confirmed by the inserted selected area diffraction pattern (SADP). However, along GBs, large primary α(Al) + θ(Al_2Cu) + S(Al_2CuMg) eutectic particles [26, 27] are found. The solute concentration profiles from the GB into the grain interior, as measured by EDX, are shown in Fig. 1b: the concentrations of alloying elements were extremely high in the matrix adjacent to the GB, especially for Cu and Mg which were measured to be about 3.1 at.% and 3.7 at.%, respectively. The concentrations of alloying elements rapidly decreased and became constant when approaching the GC: such observations are typical of an as-cast alloy ingot with dendritic segregation as seen elsewhere [26, 28].

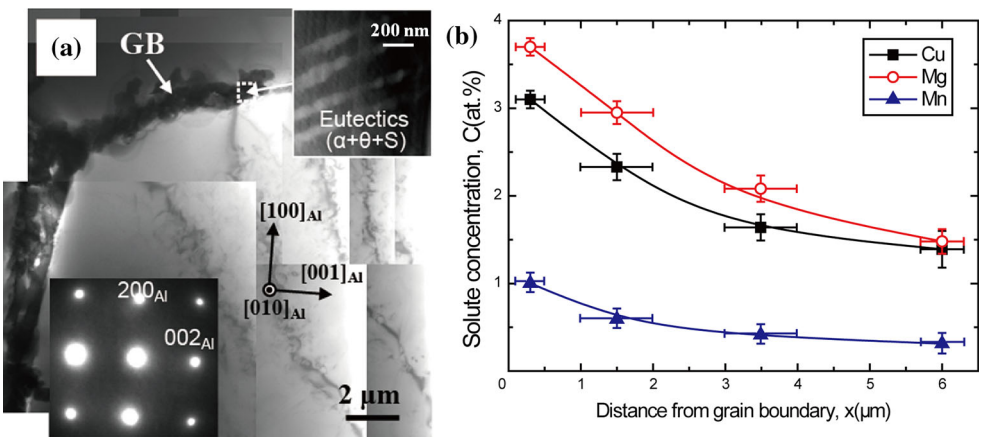

Figure 1 **a** Typical TEM micrographs and **b** concentration depth profiles of solutes (Cu, Mg, and Mn) near the GB of an as-cast Al–Cu–Mg–Mn alloy.

When the alloy was homogenised at 485 °C for 1 min, a large number of precipitates grew as laths on the {100} planes of the Al matrix as shown in Fig. 2a. Meanwhile, a PFZ with a width of 0.8 μm formed in the vicinity of the GBs. SADP revealed that these precipitates possessed an orientation relationship with the Al matrix of $[100]_P//[100]_{Al}$, $[010]_P//[02\text{-}1]_{Al}$, $[001]_P//[012]_{Al}$, with lattice parameters $a = 4.05$ Å, $b = 9.26$ Å, and $c = 7.25$ Å, which therefore can be identified as an S (Al_2CuMg) phase.

The S-phase is the main strengthening phase of this alloy, which usually forms during ageing (at 150–350 °C) [29, 30]. Previous studies showed that an S-phase can present at temperatures up to about 500 °C [19]. In the as-cast alloy, the precipitation of the S-phase at such a high temperature (485 °C) was probably due to the segregated structure (Cu and Mg solutes is highly segregated in this region).

As a result of S-phase precipitation, the solute concentrations of Cu and Mg (Fig. 2b) dropped from 3.1 to 2.8 and 3.7–3.1 at.%, respectively, in the GB-PFZ after homogenisation for 1 min; however, the deep gradients of solute concentrations inherited from casting showed little change, possibly due to the limited solute diffusion within such a short time. As can be seen in Fig. 2b, the Cu concentration in the GB-PFZ was over 50 % higher than in the precipitate-rich matrix and the Mg concentration in the GB-PFZ was also over 40 % higher than in the precipitate-rich matrix. This differed from the GB-PFZ formed during ageing where the solute concentrations were always lower in the GB-PFZ than in the precipitate-rich matrix. For example, in Hirosawa's work [12] on a binary Al–Cu alloy, the Cu concentration in the GB-PFZ was about 50 % lower than in the precipitate-rich matrix in the early stages of ageing and further increased to over 75 % in time. In Raghavan's work [13] on the GB-PFZ formation in an Al–Zn–Mg alloy, it is also shown that the Zn and Mg concentrations in the GB-PFZ were over 50 and 20 % lower than that of the precipitate-rich matrix, respectively.

With such a high supersaturated solute concentration, the GB-PFZ formed at the initial stage of homogenisation could not be contributed to any solute depletion. Thus, vacancy depletion was more likely to be the only formation mechanism for the GB-PFZ.

As homogenisation continued, the GB-PFZ quickly decreased in width. As can be seen in Fig. 3, after homogenisation at 485 °C for 10 min, S-phase particles formed closer to GB and the width of the GB-PFZ decreased significantly.

As the homogenisation time increased, the lath-shaped S-precipitates dissolved gradually and tiny rod-shaped phase particles nucleated on every single S-precipitate. After homogenisation for 30 min, the original S-precipitate finally broke up into a chain of tiny rod-shaped phase particles (Fig. 4a). Furthermore, it was worth noting that, adjacent to the GB, many rod-shaped particles formed and the GB-PFZ had completely vanished (Fig. 4b).

Figure 4c, d shows the HRTEM images of the cross sections of this rod-shaped phase, which indicated

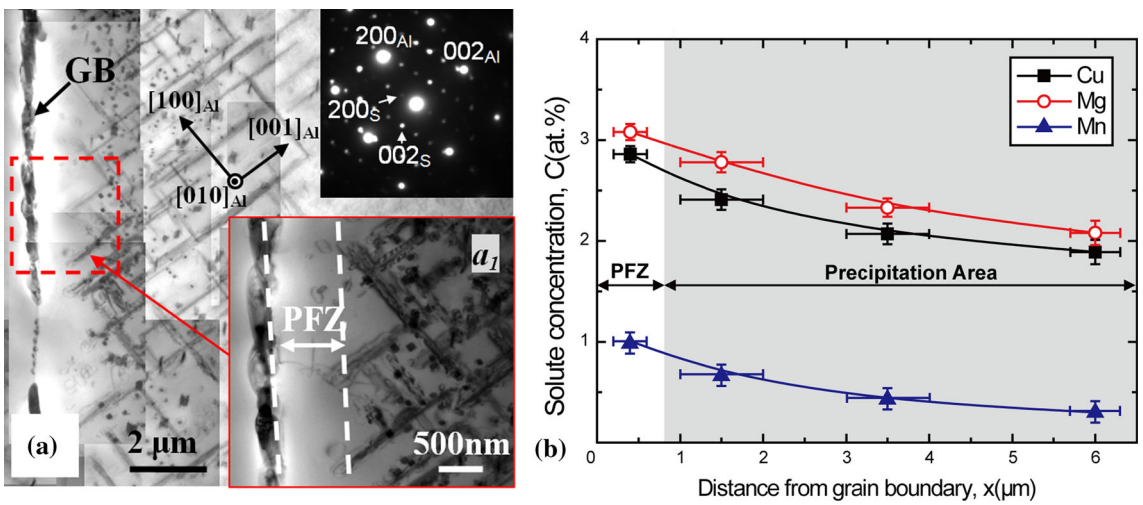

Figure 2 **a** Typical TEM micrographs and **b** concentration depth profiles of solutes (Cu, Mg, and Mn) near the GB of the Al–Cu–Mg–Mn alloy after homogenisation at 485 °C for 1 min, immediately followed by water quenching.

that these newly formed precipitates had the following lattice parameters: $a = 24.2$ Å, $b = 12.5$ Å, and $c = 7.8$ Å. The results of element mapping in Fig. 4e reveal that Cu and, in particular, Mn were highly enriched in this phase. Thus, this phase could be determined to be T ($Al_{20}Cu_2Mn_3$) phase [31], which was the main dispersoid in this alloy [32]. The precipitation of T-phase during homogenisation was mainly because of the low solubility of Mn in the Al matrix.

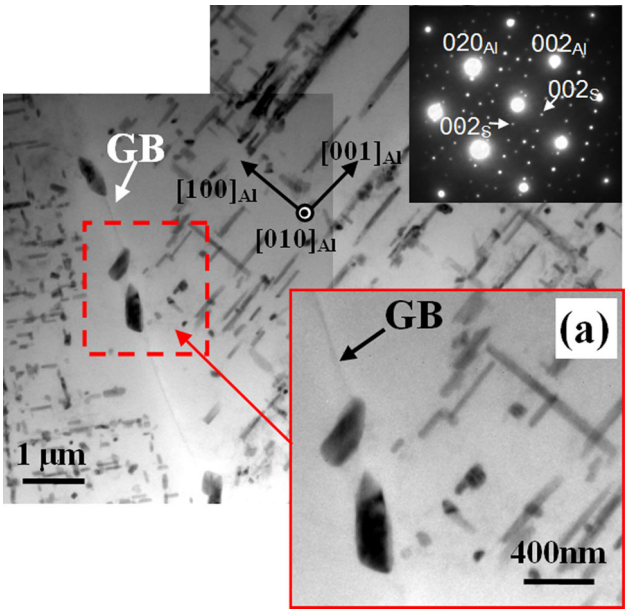

Figure 3 Typical TEM micrographs near the GB of the Al–Cu–Mg–Mn alloy after homogenisation at 485 °C for 10 min, immediately followed by water quenching, showing the S-precipitate and its further growth into the GB-PFZ.

With further homogenisation, the T-phase continued to grow and the GB-PFZ remained absent, or was extremely narrow (Fig. 5a). As can be seen in Fig. 5b, after a 1440-min homogenisation period, T-phase particles had grown to over 1 μm in diameter, and the width of GB-PFZ was less than 0.2 μm. Besides, multiple-twinned T-phase particle were found (Fig. 5c) and its composite SADP showed 10-fold symmetry (Fig. 5d), in good agreement with Feng [31].

Figure 6a, b shows the TEM micrographs and solute concentration profiles of the alloy after homogenisation at 485 °C for 6000 min. The T-phase had apparently coarsened after the long homogenisation time and more importantly, a wide PFZ was again observed in this alloy. The matrix solute concentrations from the GB into the grain interior demonstrated opposite solute concentration profiles compared to Fig. 2b. The profile showed that the

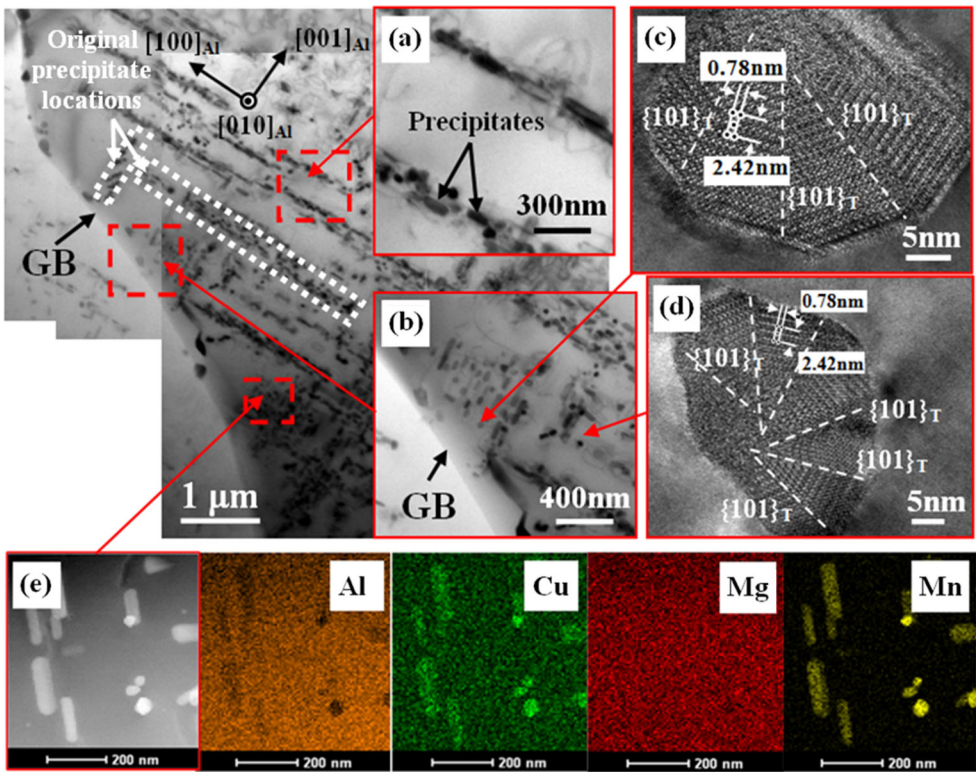

Figure 4 Microstructures near the GB of the Al–Cu–Mg–Mn alloy after homogenisation at 485 °C for 30 min, immediately followed by water quenching, showing the original S-precipitates acting as nucleation sites for the T-dispersoids.

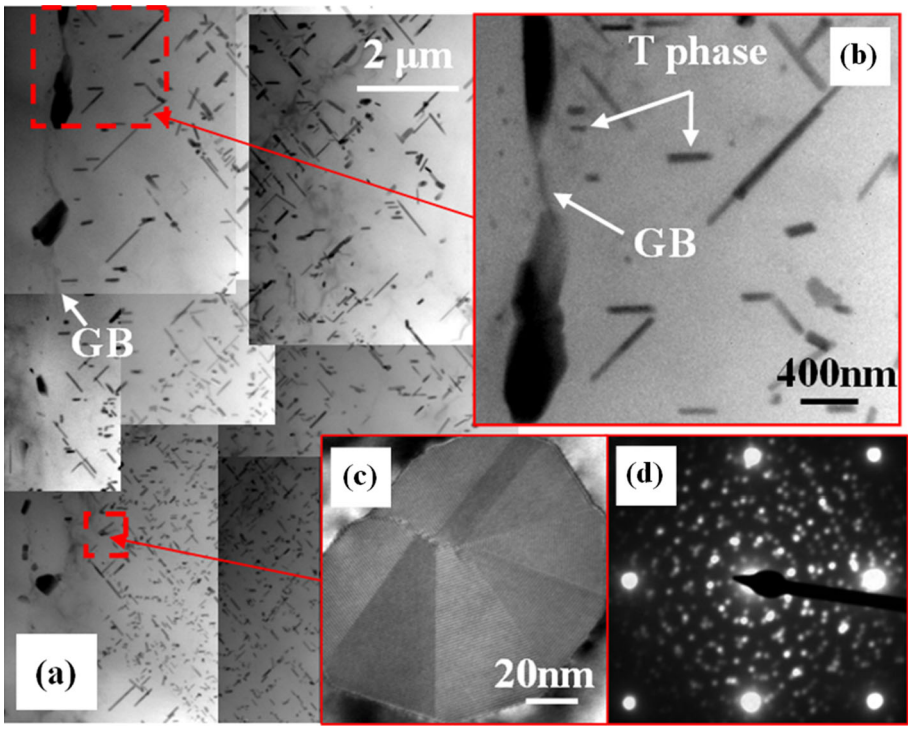

Figure 5 Microstructures near the GB of the Al–Cu–Mg–Mn alloy after homogenisation at 485 °C for 1440 min, immediately followed by water quenching.

solute concentrations were lower in the GB-PFZ than in the precipitate-rich matrix, especially for Cu and Mn. Since Cu and Mn are the major elements comprising this T-phase, the lower concentration of Cu and Mn indicated that the formation mechanism of GB-PFZ may have switched from vacancy depletion at the beginning of homogenisation to solute depletion in its later stages.

At the later stage of homogenisation, the T-phase continued to coarsen and the width of the GB-PFZ also increased. After homogenisation for 30,000 min, the width of the GB-PFZ increased to over 1 μm (Fig. 7a). The Cu and Mn concentrations in the GB-PFZ dropped to 1.1 and 0.1 at.%, respectively, which were about 35 and 65 % lower than those in the precipitate-rich matrix (Fig. 7b), suggesting solute depletion in the GB-PFZ.

The mean widths of the GB-PFZ were measured at different stages of homogenisation (Fig. 8). Unlike the GB-PFZ formed during ageing, whose width monotonically increased with ageing time, the evolution of the GB-PFZ during homogenisation could be divided into three stages.

Stage I: a wide GB-PFZ developed and narrowed gradually until vanishing when the homogenisation time reached 30 min.

Stage II: the GB-PFZ remained absent, or was extremely narrow, for homogenisation times between 30 and 1440 min.

Stage III: the GB-PFZ continued broadening with time.

Discussion

Based on the above results, a proposed precipitation process in the vicinity of GBs during homogenisation can be shown schematically in Fig. 9.

It is known that the redistribution of solutes during solidification of an alloy leads to micro-segregation of most of its elements. The distribution coefficients (C_S/C_L) of Cu and Mg elements in Al were greater than 1 [26]. Thus, during casting, the Cu and Mg concentrations in the later solidification areas were higher than those in the earlier solidification areas. In other words, the GC was purer than its sides. Therefore, a rising solute concentration profile towards the GBs could be seen (Fig. 9a). At the end of solidification, $\alpha(Al) + \theta(Al_2Cu) + S(Al_2CuMg)$ eutectics [26] form at GB due to the extremely high Cu and Mg concentrations. Assuming the later solidification areas retained fewer vacancies due to

lower solidification temperatures, a declining profile of vacancy concentration towards GB can be plotted [23, 33].

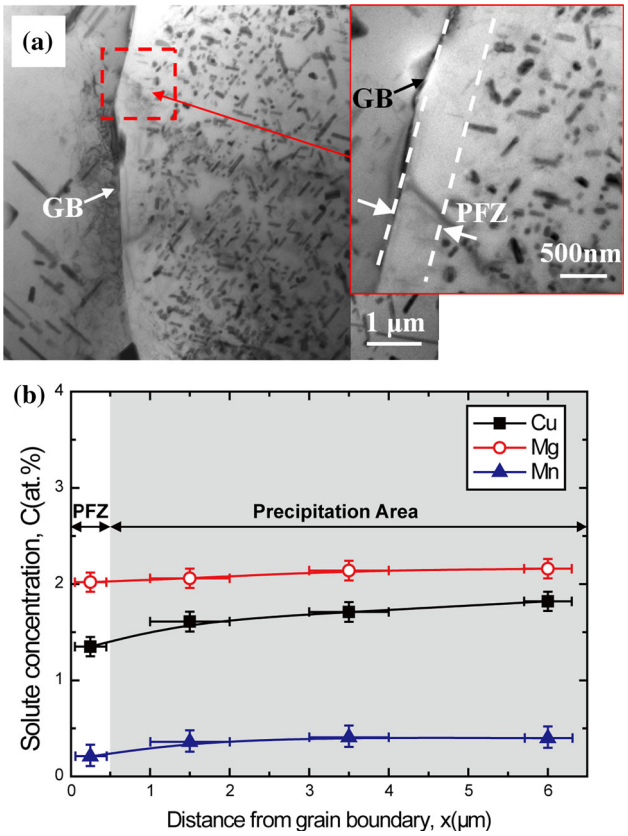

Figure 6 **a** Typical TEM micrographs and **b** concentration depth profiles of solutes (Cu, Mg, and Mn) near the GB of the Al–Cu–Mg–Mn alloy after homogenisation at 485 °C for 6000 min, immediately followed by water quenching.

As homogenisation starts, a large number of lath-shaped S-phase particles quickly precipitated out. The driving force for S-phase precipitation was the local supersaturation of Cu and Mg. While in the matrix close to the GB (up to 0.8 μm from it), no S-phase precipitation was found and a wide PFZ formed (Fig. 9b). The formation mechanism of this GB-PFZ was different from that formed during ageing.

Before ageing, the as-quenched alloy after solution treatment exhibited a uniform solute distribution from grain-to-grain across the GBs [34, 35]. Once ageing starts, the preferential precipitation at GBs grabbed solutes from nearby regions and inevitably

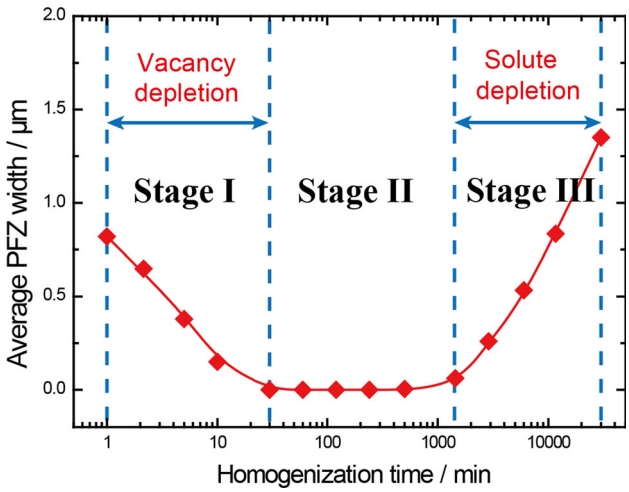

Figure 8 Change in GB-PFZ width during the homogenisation of an Al–Cu–Mn–Mg alloy at 485 °C.

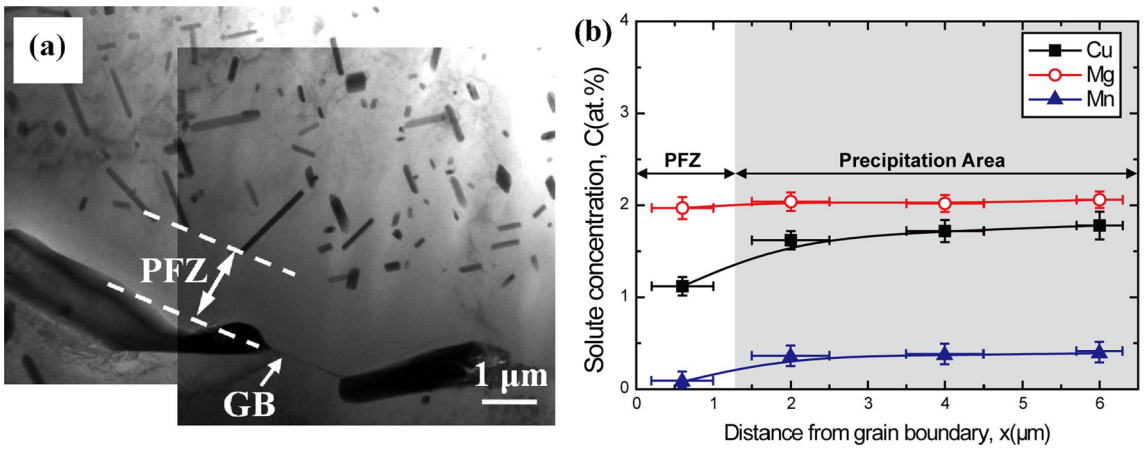

Figure 7 **a** Typical TEM micrographs and **b** concentration depth profiles of solutes (Cu, Mg, and Mn) near the GB of the Al–Cu–Mg–Mn alloy after homogenisation at 485 °C for 30,000 min, immediately followed by water quenching.

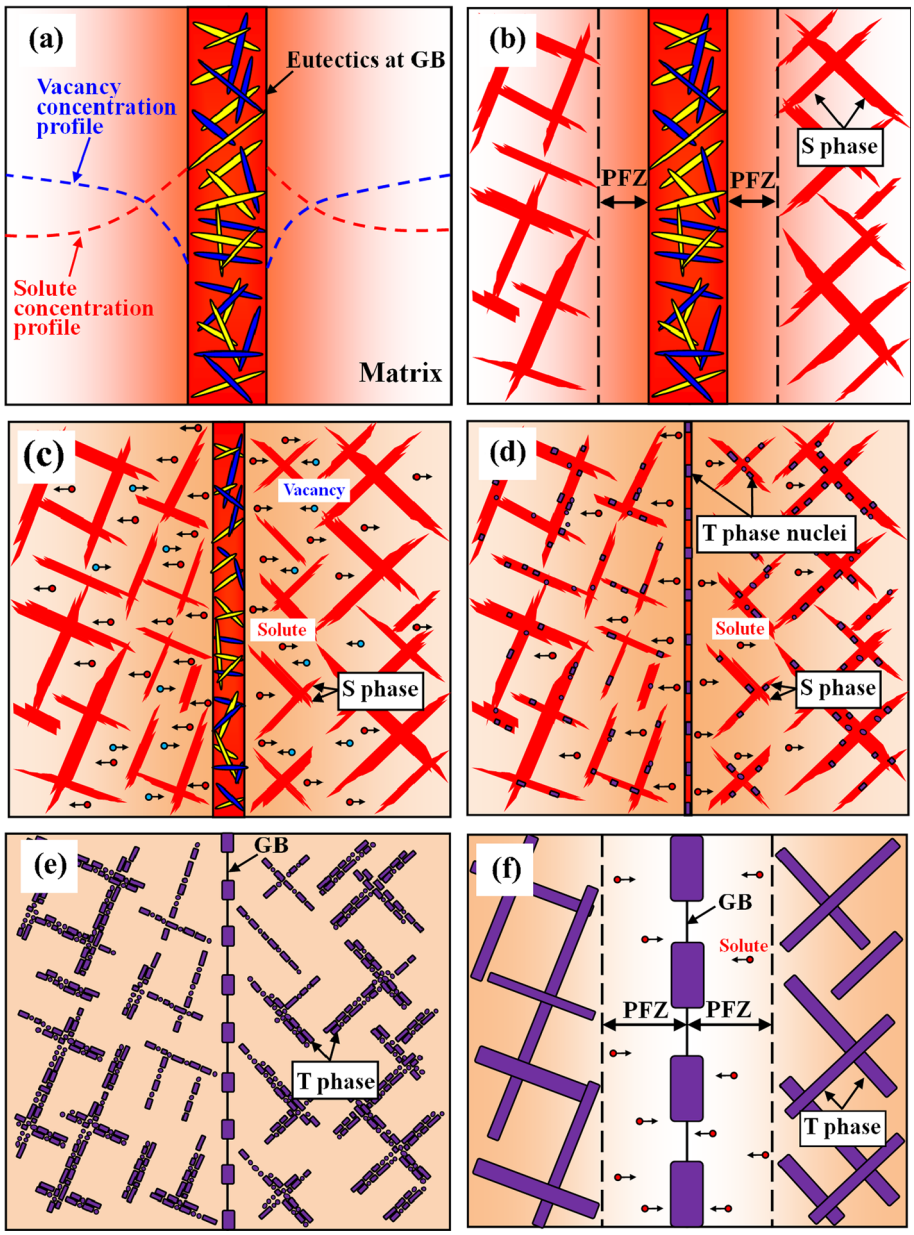

Figure 9 Schematic illustration of PFZ evolution in Al–Cu–Mg alloy during homogenisation **a** as-cast condition **b** formation of S-precipitates and GB-PFZ **c** narrowing of GB-PFZ caused by the rising vacancy concentration **d** the heterogeneous nucleation of T-dispersoids on the S-precipitates **e** S-precipitates completely dissolving **f** re-formation and broadening of GB-PFZ.

produced a declining solute profile from GC to GB in the region adjacent to the GB. In other words, in the GB-PFZ formation during ageing, solute depletion could ever exist. For example, in Tolley's work [17] on PFZ formation in an Al–Cu Alloy during ageing, it was found that a certain level of Cu solute depletion occurred at the beginning of GB-PFZ formation and the solute depletion became more obvious in time.

Before homogenisation, in the as-cast alloy, the solutes were highly segregated towards the GBs. It produced a sharply rising profile of matrix solute concentrations from GC to GB. Even though the matrix solute concentrations next to GBs decreased to a certain extent due to precipitation, they were still apparently greater than those far from the GBs, due to the original local high solute concentrations inherited from casting. As can be seen in Fig. 2b, the matrix solute concentrations were much higher in GB-PFZ than those in precipitation areas. Therefore, this PFZ formation was unlikely to be attributable to solute depletion. Since a critical vacancy concentration was required for the nucleation of precipitates [36] and a rising profile of vacancy concentration from GB to GC was anticipated, this PFZ formation was only be led by vacancy depletion (Stage I).

Since the homogenisation temperature was high (485 °C) and was close to that used for solution

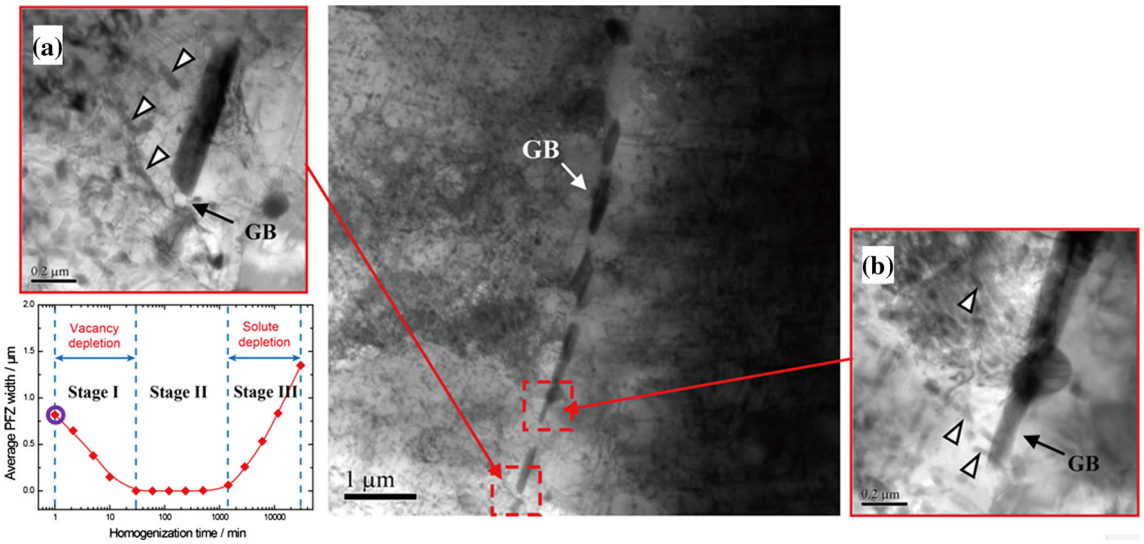

Figure 10 TEM images of a sample homogenised at 485 °C for 1 min, cold rolling to about 10 % deformation, and rehomogenised at 485 °C for 1 min.

Figure 11 TEM images of a sample homogenised at 485 °C for 14,400 min, cold rolling to about 10 % deformation, and rehomogenised at 485 °C for 1 min.

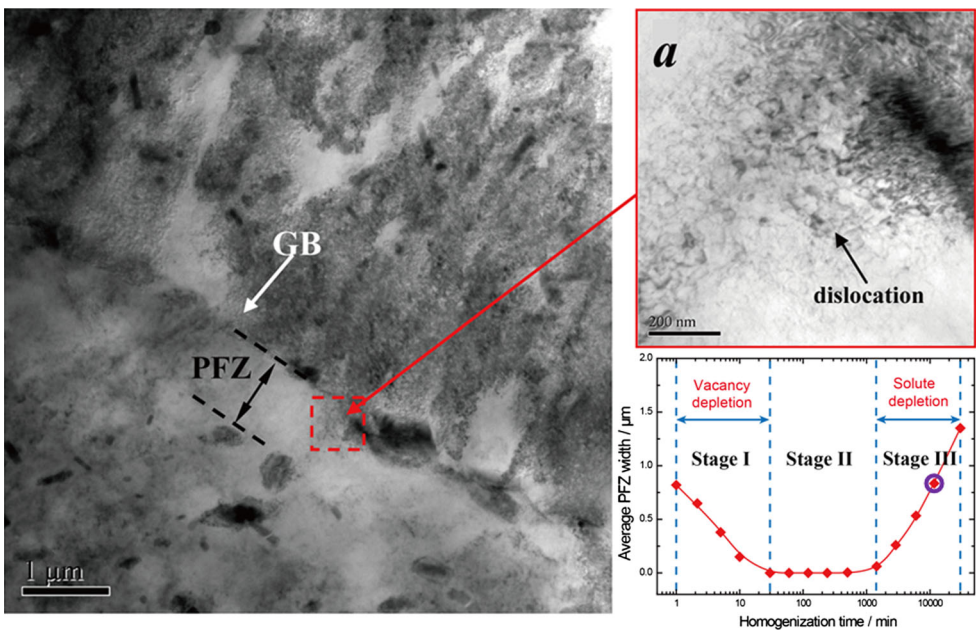

treatment (e.g. 500 °C), the equilibrium vacancy concentration under homogenisation was significantly higher than that under ageing conditions which were sufficient for precipitate nucleation. As the homogenisation starts, the vacancy concentration in the matrix gradually increased with increasing temperature. As a consequence, precipitation gradually occurred further inside the GB-PFZ where there was solute enrichment but vacancy depletion. Thus, the GB-PFZ became narrower with increasing homogenisation time, and finally disappeared (Fig. 9c).

In Al alloys, homogenisation was performed to redistribute the solutes and dissolve any unwanted eutectic phases [37]. Thus, during homogenisation, on one hand, the solutes were transported from the GB to GC by the diffusion. On the other hand, the non-equilibrium state eutectic particles at the GB dissolved gradually and release solutes into the matrix near each GB [38]. As a result, a high level of

solute concentration would remain for a certain (relatively long) time during homogenisation. The vacancy concentration increased with temperature at the beginning of homogenisation, and quickly reached, and remained at, a high level (the equilibrium value). Therefore, there existed a period of time when the solute concentration was at the same level as the vacancy concentration. In this period, the GB-PFZs remained absent in the alloy (Stage II).

As homogenisation continued, the soluble eutectics content decreased and the matrix solute concentration gradients decreased gradually due to the atomic diffusion. After a certain homogenisation time, the S-phase precipitated during the initial stage of homogenisation redissolved, since the solute concentrations had been reduced to a value below which the S-phase was unstable.

Since Mn had a low solubility in Al, it precipitated out as the T-dispersoid during the homogenisation of this alloy. Unlike the precipitates, the dispersoids were resistant to dissolution and could control the evolution of both grain and sub-grain, structures during subsequent processing [39, 40], such as hot rolling and solution heat treatment [41]. The diffusion of Mn was much slower compared with that of Mg and Cu [42]; therefore, the precipitation of the T-dispersoid was much more sluggish than that of the S-precipitate.

The T-dispersoids contained Cu atoms and a critical Cu concentration was probably required for the T-dispersoids to nucleate. Since the S-phase and the T-phase shared the same phase-forming element in Cu, the T-dispersoids were prone to heterogeneous nucleation on the dissolving S-precipitates where the Cu atom was enriched (Fig. 9d). This agreed the investigations by Lodgaard et al. [43] and Hirasawa et al. [44], which indicated that pre-existing precipitates often act as nucleation sites for Mn-containing dispersoids. The heterogeneously nucleated T-dispersoid will consume the S-precipitate completely (Fig. 9e) and gradually coarsens with increasing homogenisation time, as predicted by Ostwald ripening theory.

During homogenisation, the concentration gradients of solutes reduced as a consequence of atomic diffusion [45, 46] and eventually the concentration difference of solutes in the matrix should be equalised. Then, due to a more rapid coarsening of T-dispersoids at GBs, the matrix solute concentrations near the GBs became lower than that at the GC, and the GB-PFZs reform and developed gradually (Fig. 9f).

It should be emphasised that the GB-PFZ formed during the later stage of homogenisation was also different from that formed during ageing. In ageing conditions, due to the precipitation, the number of excess vacancies retained by quenching continued to decrease. Thus, it is difficult to tell whether vacancy depletion assisted GB-PFZ formation, in particular, during late-stage ageing. However, under homogenisation conditions, owing to the high holding temperature, the vacancy concentration rapidly approached, and remained at a high level. Therefore, the vacancy depletion was not likely to have been the cause of the GB-PFZ formation in late-stage homogenisation, but solute depletion (Stage III) was.

It is known that if the PFZ is vacancy depleted but solute supersaturated, precipitation can be induced by introducing lattice imperfections by deformation [13]. Therefore, samples homogenised for 1 min (Stage I), and 14,400 min (Stage III) were deformed 10 % at room temperature and then rehomogenised for 1 min at 485 °C to determine whether or not heterogeneous nucleation of precipitates could be induced in the PFZ.

Figure 10 shows the bright-field images of a sample homogenised for 1 min at 485 °C, deformed by 10 %, and rehomogenised at 485 °C for 1 min. As can been seen, after the second homogenisation treatment, quantities of second phase (as indicated by white triangles) heterogeneously precipitated on the dislocation lines in the initial GB-PFZ due to the high degree of solute supersaturation. For the sample homogenised for 14,400 min at 485 °C, deformed by 10 %, and rehomogenised at 485 °C for 1 min (Fig. 11), although many dislocations were induced by deformation, no second phase formed in the initial GB-PFZ due to the low solute concentrations. This confirmed that the GB-PFZ formed in Stage I was led by vacancy depletion, while the GB-PFZ formed in Stage III was attributed to solute depletion.

It should be noted that the homogenisation temperature of 485 °C is apparently higher than those temperatures commonly used for the annealing of this alloy (250–350 °C) [47, 48]. At such a high temperature, on one hand, the number of dislocations would decrease rapidly due to the annihilation of dislocations caused by recovery. On the other hand, the heterogeneous nucleation of second-phase

particles on dislocations could also take place rapidly under conditions of local solute supersaturation. Thus, when the deformed alloy is homogenised, there is a competition between the annihilation of dislocations and the heterogeneous nucleation on the dislocations.

Dislocation annihilation is known to be a time-consuming process, which includes glide, climb, and cross-slip of dislocations [49]. In Michalcová's work on microstructural evolution upon annealing of an Al–Fe–Cr–Ce alloy [50], it is shown that, after cold rolling and annealing at 400 °C for 100 h, a high density of dislocations were still present in the matrix. Similar results were observed by Zeng [51] on an AA 3004 Al alloy after annealing at 420 °C for 3 h. Particularly, in Al alloys with a large number of second-phase particles, the process of dislocation annihilation was retarded, since the these particles have a strong pinning effect on dislocation motion. Lucadamo's work [52] on a 5083 Al alloy revealed that, even after annealing at 500 °C for 2 h, a high density of dislocations surrounding precipitates was still observed. In this study, the retention of dislocations after homogenisation is probably due to the limited homogenisation time (1 min) and the pinning effect of second-phase particles on dislocations.

The heterogeneous nucleation of second-phase particles on dislocations is widely observed in Al alloys not only during ageing but also during homogenisation. For instance, in Tsivoulas's work [53] on the homogenisation of an Al–Cu–Li-Zr-Mn alloy, it is revealed that the Al_3Zr and T($Al_{20}Cu_2Mn_3$) phases had a strong tendency to undergo heterogeneous nucleation on dislocations. Similar heterogeneous precipitation is also reported by Marquis [54] in Al–Sc alloys during homogenisation. Furthermore, Robson [55] concluded that a high dislocation density can increase the frequency of heterogeneous precipitation of Al_3Zr dispersoids.

Solute segregation at dislocations was thought to be the key reason for this heterogeneous nucleation, since it produces a high level of local supersaturation. Likewise, the Cu segregation at dislocations should respond to the heterogeneous nucleation of second-phase particles in this alloy (both S-precipitates and T-dispersoids contain Cu). In Al alloys, the Cu atom is sensitive to dislocation, since it has a much smaller radius (0.128 nm) than that of Al (0.182 nm) [56]. After deformation, to release local compressive stress, Cu atoms are prone to gather along dislocation lines, which results in the segregation of Cu atoms at dislocations (this gathering effect of Cu atoms in Al–Cu–Mg–Mn alloys has already been proved elsewhere [57, 58]). During homogenisation, even though some dislocations were quickly annihilated, the local solute segregation at dislocations was retained, which provided a large number of heterogeneous nucleation sites for second-phase precipitation.

Conclusions

The microstructural evolution and solute distributions in the vicinity of GBs during homogenisation at 485 °C were investigated in an Al–Cu–Mg–Mn alloy. The main conclusions are summarised as follows:

1. Quantities of S-precipitates formed rapidly at the edge of each grain due to local high solute concentrations induced by micro-segregation. As a consequence of atomic diffusion, this micro-segregation gradually disappeared and the S-precipitates were finally replaced by T-dispersoids.
2. A wide GB-PFZ featuring extremely high solute concentrations formed within 1 min of homogenisation, and decreased in thickness with increasing homogenisation time. The GB-PFZ was absent within homogenisation times between 30 and 1440 min, after which the GB-PFZ reappeared and broadened.
3. The early stage of GB-PFZ formation was exclusively led by vacancy depletion, while the later stage of GB-PFZ formation was solely attributed to solute depletion.

Acknowledgements

This work was supported by the National Natural Science Foundation of China (Grant Nos. 51405153 and 51475162) and by funds from the Major State Basic Research Projects of China (Grant No. 2012CB619506). We also thank Dr L.X. Wang and S.C. Li for their helpful discussion about this research.

References

[1] Chen JH, Costan E, Huis MA, Xu Q, Zandbergen HW (2006) Atomic-pillar-based nanoprecipitates strengthen AlMgSi alloys. Science 312:416–419

[2] Chrominski W, Lewandowska M (2016) Precipitation phenomena in ultrafine grained Al–Mg–Si alloy with heterogeneous microstructure. Acta Mater 103:547–557

[3] Lin YC, Zhang J, Liu G, Liang Y (2015) Effects of pretreatments on aging precipitates and corrosion resistance of a creep-aged Al–Zn–Mg–Cu alloy. Mater Des 83:866–875

[4] Liu SD, Chen B, Li CB, Dai Y, Deng YL, Zhang XM (2015) Mechanism of low exfoliation corrosion resistance due to slow quenching in high strength aluminium alloy. Corros Sci 91:203–212

[5] Liu H, Qiao X, Chen Z, Jiang R, Li X (2011) Effect of ultrasonic vibration during casting on microstructures and properties of 7050 aluminum alloy. J Mater Sci 46:3923–3927

[6] Lütjering G, Albrecht J, Sauer C, Krull T (2007) The influence of soft, precipitate-free zones at grain boundaries in Ti and Al alloys on their fatigue and fracture behavior. Mater Sci Eng, A 468–470:201–209

[7] Xu DK, Rometsch PA, Li L, Shen LM, Birbilis N (2014) Critical conditions for the occurrence of quench cracking in an Al–Zn–Mg–Cu alloy. J Mater Sci 49:4687–4697

[8] Lin YC, Xia Y, Jiang Y, Zhou H, Li L (2013) Precipitation hardening of 2024-T3 aluminum alloy during creep aging. Mater Sci Eng, A 565:420–429

[9] Morgeneyer TF, Starink MJ, Wang SC, Sinclair I (2008) Quench sensitivity of toughness in an Al alloy: direct observation and analysis of failure initiation at the precipitate-free zone. Acta Mater 56:2872–2884

[10] Krol T, Baither D, Nembach E (2004) The formation of precipitate free zones along grain boundaries in a superalloy and the ensuing effects on its plastic deformation. Acta Mater 52:2095–2108

[11] Okuda H, Ochiai S (2004) The effects of solute and vacancy depletion on the formation of precipitation-free zone in a model binary alloy examined by a Monte Carlo simulation. Mater Trans 45:1455–1460

[12] Hirosawa S, Oguri Y, Sato T (2005) Experimental and computational investigation of formation of precipitate free zones in an Al–Cu alloy. Mater Trans 46:1230–1234

[13] Raghavan M (1980) Microanalysis of precipitate free zones (PFZ) in Al–Zn–Mg and Cu–Ni–Nb alloys. Metall Trans A 11:993–999

[14] Shastry CR, Judd G (1972) An electron microprobe analysis of solute segregation near grain boundaries in an Al–Zn–Mg alloy. Metall Trans 3:779–782

[15] Ogura T, Hirosawa S, Sato T (2004) Quantitative characterization of precipitate free zones in Al–Zn–Mg(–Ag) alloys by microchemical analysis and nanoindentation measurement. Sci Technol Adv Mater 5:491–496

[16] Hirosawa S, Sato T, Kamio A, Flower HM (2000) Classification of the role of microalloy elements in phase decomposition of Al based alloys. Acta Mater 48:1797–1806

[17] Tolley A, Mitlin D, Radmilovic V, Dahmen U (2005) Transmission electron microscopy analysis of grain boundary precipitate-free-zones (PFZs) in an AlCuSiGe alloy. Mater Sci Eng, A 412:204–213

[18] Okuda H, Ochiai S (2005) A Monte Carlo simulation on the PFZ microstructures in Al-based alloys during multistep annealing. Mater Sci Forum 475–479:937–940

[19] Starink MJ, Gregson PJ (1996) S′ and δ′ phase precipitation in SiCp reinforced A1-1.2 wt%Cu -1 wt% Mg-x Li alloys. Mater Sci Eng, A 211:54–65

[20] Starink MJ, Wang P, Sinclair I, Gregson PJ (1999) Microstrucure and strengthening of Al–Li–Cu–Mg alloys and MMCs: II. Modelling of yield strength. Acta Mater 47:3855–3868

[21] Cai M, Robson JD, Lorimer GW (2007) Simulation and control of dispersoids and dispersoid-free zones during homogenizing an AlMgSi alloy. Scripta Mater 57:603–606

[22] Gandin CA, Jacot A (2007) Modeling of precipitate-free zone formed upon homogenization in a multi-component alloy. Acta Mater 55:2539–2553

[23] Chen YQ, Yi DQ, Jiang Y, Wang B, Liu HQ (2013) Concurrent formation of two different type precipitation-free zones during the initial stage of homogenization. Philos Mag 93:2269–2278

[24] Park JK, Ardell AJ (1992) Solute-enriched surface layers and X-ray microanalysis of thin foils of a commercial aluminium alloy. J Microsc 165:301–309

[25] Lorimer GW, Cliff G, Clark JN (1976) Developments in electron microscopy and analysis. Academic Press, London

[26] Xie FY, Kraft T, Zuo Y, Moon CH, Chang YA (1999) Microstructure and microsegregation in Al rich Al–Cu–Mg alloys. Acta Mater 47:489–500

[27] Norman AF, Hyde K, Costello F, Thompson S, Birley S, Prangnell PB (2003) Examination of the effect of Sc on 2000 and 7000 series aluminium alloy castings: for improvements in fusion welding. Mater Sci Eng, A 354:188–198

[28] McPhee WAG, Schaffer GB, Drennan J (2003) The effect of iron on liquid film migration and sintering of an Al–Cu–Mg alloy. Acta Mater 51:3701–3712

[29] Wang SB, Chen JH, Yin MJ, Liu ZR, Yuan DW, Liu JZ, Liu CH, Wu CL (2012) Double-atomic-wall-based dynamic precipitates of the early-stage S-phase in AlCuMg alloys. Acta Mater 60:6573–6580

[30] Liu ZR, Chen JH, Wang SB, Yuan DW, Yin MJ, Wu CL (2012) The structure and the properties of S-phase in AlCuMg alloys. Acta Mater 59:7396–7405

[31] Feng ZQ, Yang YQ, Huang B, Li MH, Chen YX, Ru JG (2014) Crystal substructures of the rotation-twinned T (Al20Cu2Mn3) phase in 2024 aluminum alloy. J Alloys Compd 583:445–451

[32] Wang J, Zhang B, Zhou YT, Ma XL (2015) Multiple twins of a decagonal approximant embedded in S-Al2CuMg phase resulting in pitting initiation of a 2024 Al alloy. Acta Mater 82:22–31

[33] Ogura T, Hirosawa S, Cerezo A, Sato T (2010) Atom probe tomography of nanoscale microstructures within precipitate free zones in Al–Zn–Mg(–Ag) alloys. Acta Mater 58:5714–5723

[34] Yukawa H, Urata Y, Morinaga M, Takahashi Y, Yoshida H (1995) Heterogeneous distributions of magnesium atoms near the precipitate in Al–Mg based alloys. Acta Metal Mater 43:681–688

[35] Hass M, Hosson JTM (2001) Grain boundary segregation and precipitation in aluminum alloys. Scripta Mater 44:281–286

[36] Macchi CE, Somoza A, Dupasquier A, Polmear IJ (2003) Secondary precipitation in Al–Zn–Mg–(Ag) alloys. Acta Mater 51:5151–5158

[37] Dons AL (2001) The Alstruc homogenization model for industrial aluminum alloys. J Light Met 1:133–149

[38] Yan L, Zhang Y, Li X, Li Z, Wang F, Liu H, Xiong B (2014) Microstructural evolution of Al-0.66 Mg-0.85Si alloy during homogenization. Trans Nonferrous Met Soc China 24:939–945

[39] Chen YQ, Yi DQ, Jiang Y, Wang B, Xu DZ, Li SC (2013) Twinning and orientation relationships of T-phase precipitates in an Al matrix. J Mater Sci 48:3225–3231

[40] Wang SC, Starink MJ (2005) Precipitates and intermetallic phases in precipitation hardening Al–Cu–Mg–(Li) based alloys. Int Mater Rev 50:193–215

[41] Chen YQ, Pan SP, Zhou MZ, Yi DQ, Xu DZ, Xu YF (2013) Effects of inclusions, grain boundaries and grain orientations on the fatigue crack initiation and propagation behavior of 2524-T3 Al alloy. Mater Sci Eng, A 580:150–158

[42] Wu Y, Xiong J, Lai R, Zhang X, Guo Z (2009) The microstructure evolution of an Al–Mg–Si–Mn–Cu–Ce alloy during homogenization. J Alloys Compd 475:332–338

[43] Lodgaard L, Ryum N (2000) Precipitation of dispersoids containing Mn and/or Cr in Al–Mg–Si alloys. Mater Sci Eng, A 283:144–152

[44] Hirasawa H (1975) Precipitation process of Al-Mn and Al-Cr supersaturated solid solution in presence of age hardening phases. Scripta Metall 9:955–958

[45] Liu Y, Jiang D, Xie W, Hu J, Ma B (2014) Solidification phases and their evolution during homogenization of a DC cast Al–8.35Zn–2.5 Mg–2.25Cu alloy. Mater Charact 93:173–183

[46] Jia M, Zheng Z, Gong Z (2014) Microstructure evolution of the 1469 Al–Cu–Li–Sc alloy during homogenization. J Alloys Compd 614:131–139

[47] Shen F, Yi D, Jiang Y, Wang B, Liu H, Tang C, Shou W (2016) Semi-quantitative evaluation of texture components and fatigue properties in 2524 T3 aluminum alloy sheets. Mater Sci Eng, A 657:15–25

[48] Alil A, Popović M, Radetić T, Zrilić M, Romhanji E (2015) Influence of annealing temperature on the baking response and corrosion properties of an Al–4.6 wt% Mg alloy with 0.54 wt% Cu. J Alloys Compd 625:76–84

[49] Humphreys FJ, Hatherly M (2004) Recrystallization and related annealing phenomena. Elsevier Ltd, Amsterdam

[50] Michalcová A, Vojtěch D, Čížek J, Procházka I, Drahokoupil J, Novák P (2011) Microstructure characterization of rapidly solidified Al–Fe–Cr–Ce alloy by positron annihilation spectroscopy. J Alloys Compd 509:3211–3218

[51] Zeng Q, Wen X, Zhai T (2009) Effect of precipitates on the development of P orientation $011 < 566 >$ in a recrystallized continuous cast AA 3004 aluminum alloy after cold rolling. Metall Mater Trans A 40:2488–2497

[52] Lucadamo G, Yang NYC, Marchi CS, Lavernia EJ (2006) Microstructure characterization in cryomilled Al 5083. Mater Sci Eng, A 430:230–241

[53] Tsivoulas D, Robson JD (2015) Heterogeneous Zr solute segregation and Al3Zr dispersoid distributions in Al–Cu–Li alloys. Acta Mater 93:73–86

[54] Marquis EA, Seidman DN (2001) Nanoscale structural evolution of Al3Sc precipitates in Al(Sc) alloys. Acta Mater 49:1909–1919

[55] Robson JD, Jones MJ, Prangnell PB (2003) Extension of the N-model to predict competing homogeneous and heterogeneous precipitation in Al–Sc alloys. Acta Mater 51:1453–1468

[56] Matsuda K, Ikeno S, Sato T, Uetani Y (2006) New quaternary grain boundary precipitate in Al–Mg–Si alloy containing silver. Scripta Mater 55:127–129

[57] Huang YJ, Chen ZG, Zheng ZQ (2011) A conventional thermo-mechanical process of Al–Cu–Mg alloy for increasing ductility while maintaining high strength. Scripta Mater 64:382–385

[58] Yin D, Xiao Q, Chen Y, Liu H, Yi D, Wang B, Pan S (2016) Effect of natural ageing and pre-straining on the hardening behaviour and microstructural response during artificial ageing of an Al–Mg–Si–Cu alloy. Mater Des 95:329–339